1 **REVISION 2**

2 **TITLE 1**

3 **The effect of XPS background removing method on the appraisal of Ti and Fe: the case of**

4 **phlogopites and brookite**

5

6 M. R. Guascito[1], E. Mesto[2], C. Malitesta[1], R. Picca[1], F. Scordari[2]

7

8 [1]Dipartimento di Scienze e Tecnologie Biologiche e Ambientali, Università del Salento, via

9 Monteroni, 73100 Lecce, Italy

10 [2]Dipartimento di Scienze della Terra e Geoambientali, Università degli Studi di Bari "Aldo Moro",

11 via E. Orabona 4, 70125 Bari, Italy

12

13

14

15
16

17

18

19

20

21

22

23 submitted to:
24 word processor: *Word Microsoft Office 2010*
25 address of the corresponding author:
26 Dr. E. Mesto
27 Dipartimento di Scienze della Terra e Geoambientali, Università degli Studi di Bari
28 Via Orabona 4, I-70125 Bari, Italy
30 e-mail: ernesto.mesto@uniba.it

31   **ABSTRACT**

32   The determination of the oxidation state and structural role of transition metals in minerals,

33   especially when carried out on single crystal, is nowadays a crucial challenge. XPS has proven to

34   have a great potential in probing the site distribution and chemical states of Fe and Ti transition

35   elements, provided that the right method to process the spectra is used. XPS spectrum of these

36   elements have the $2p$ core level region usually rich of features but the choice of the method for the

37   background removing can seriously affect the results of the quantitative analysis. Single crystal of

38   brookite (TiO_2) and natural micas (phlogopites) are investigated in order to examine the effect of

39   background subtraction on Ti2p and Fe2p signals. The backgrounds used are (i) the "Linear"

40   background, (ii) the traditional "Shirley" background, (iii) three different Tougaard-like

41   backgrounds and (iv) the more recent "Shape parameter, κ" method. In the case of the studied

42   natural micas, the Fe chemical state proportion (Fe^{2+}/Fe_{tot}) obtained with the corrected spectra

43   varies by 10%. It is shown that TiO_2 oxides are not suitable as standard for octahedral Ti^{4+} signal in

44   the studied micas The "shape parameter, κ" method proves to provide supplementary information

45   useful for a full interpretation of XPS signals.

46

47   **Keywords:** XPS, background subtraction, Fe,Ti-oxidation state, mica, brookite

48

49

INTRODUCTION

50

51   It is known that natural micas are ubiquitous minerals stable in a wide range of petrogenitc

52 conditions. The peculiar structural features allow them to respond to changes in physico-chemical

53 conditions by adjusting the tetrahedral sheet as a function of the octahedral sheet cation site

54 population. As consequence, in principles micas are able to record in their structure, information

55 about the geologic history their host rock underwent (Henry and Guidotti, 2002; Cesare et al., 2003;

56 Henry et al., 2005). In order to extract the petrologic information which is in micas, the

57 determination of a reliable structural formula is a fundamental step. However, this result largely

58 depends on an accurate determination of oxidation states and structural roles of Fe and Ti, often

59 copresent in the same mica crystal. Actually, the knowledge of the site population and the chemical

60 states of Ti and Fe in minerals is of paramount importance to gain information about the parameters

61 that drive the mineral crystallization (Kühberger et al., 1989) but, unfortunately, when these two

62 elements occurred at the same time the determination of their speciation is often problematic.

63   As known, Mössbauer technique is the most used method to investigate Fe in such

64 minerals, but the interpretation of sub-spectral components in Mössbauer spectra proved to be very

65 complicated when the analysis is carried out on single crystals (Dyar, 2000). The investigation of Ti

66 by spectroscopic methods resulted in ambiguous conclusions about its oxidation state and

67 crystallographic location. As consequence, the full characterization of transition elements,

68 especially Ti, in mica still today, is a matter of debate. Actually, the study is quite complicated

69 because UV-VIS spectroscopy (Hawthorne, 1988) leads to misleading results. Waychunas (1987)

70 examined the near K-edge X-ray absorption spectra of Ti in a suite of silicate and oxide minerals in

71 order to improve Ti characterization in solids, concluding that tetrahedral Ti^{4+} probably occurs only

72 at very small concentration levels in silicates, even when the total Si^{4+} and Al^{3+} concentration is

73 well below that necessary to fill tetrahedral position as in the melanite-schorlomite garnets. The

74 levels of Ti^{3+} are more difficult to determine because of an apparent sensitivity of the pre-edge Ti^{4+}

75 features to bulk chemistry. However, the overall results seems to be consistent with only small

76   amounts of Ti^{3+}, even in sample from localities where other analyses (wet chemical and Mössbauer)

77   indicated significant Ti^{3+} amount. Rager et al., 2003 attempted a full characterization of the Ti^{3+}

78   oxidation state in a synthetic pyrope single crystal by means of electron paramagnetic resonance

79   (EPR) measurements. Based on the composition of the pyrope, its known structure and the EPR

80   spectrum results, they suggested small concentrations of Ti^{3+} at the octahedral site. In addition,

81   taking into account the previously published optical absorption measurements and microprobe

82   analysis, the same authors concluded that the most of the octahedral Ti were in the oxidation state

83   (IV). Malitesta et al. (1995) used X-ray photoelectron spectroscopy (XPS) to investigate the

84   oxidation state and structural role of Ti and Fe in melanites. The authors fitted the Ti2p photopeak

85   using the line parameters obtained by XPS investigation carried out on some Ti oxide standards.

86   Their results showed the presence of three Ti species, among which the occurrence of Ti^{3+} is

87   noteworthy.

88   XPS technique can be a very useful tool in studying mineral matrices (Seyama and Soma,

89   1985), especially as to Ti and Fe, because the chemical shifts of these elements is related to their

90   oxidation state and chemical environment (Marabini et al., 1993 and reference therein). As well

91   known, in the interpretation of XPS spectra, particularly in terms of speciation, the "secondary

92   structures" like shake-up, plasmon-loss, intrinsic and extrinsic losses (background), and the Auger

93   parameter play an important role (Castle and Salvi., 2001a; Tam et al., 2012). Therefore, a reliable

94   XPS study of chemical states, especially with quantitative aims, needs an accurate analysis of

95   photoelectron spectrum. In this process two steps are particularly sensible: firstly, the removing of

96   energy loss background by means of an algorithm which subtracts the electron inelastic scattering

97   component and secondly the curve fit of the enveloped photopeak in order to solve the overlapping

98   of chemical states. In particular for transition metals, XPS spectra result to be rather complex and

99   extreme care should be used when these steps are performed.

100   In this work, the study of the 2p region of Ti and Fe acquired on single crystal of two

101   different kinds of natural micas (phlogopites) and brookite (TiO_2) has been presented, paying

102   special attention to the influence of background removing on the results of determination of their

103   chemical states and their proportions. In particular, the Ti2p region present in oxide systems, both

104   natural and synthetic, and in two natural micas from two different geological contests has been

105   studied. For these latters also the region of Fe2p was analysed.

106   Six different background subtraction methods have been applied to experimental spectra in

107   order to study their effect on the qualitative and quantitative determination of Fe and Ti ions. The

108   compared methods are: *i*) the "Linear" background (Ghosh and Sreemany,1993); *ii*) two kind of

109   Shirley backgrounds, the classic one (Shirley, 1972) and the recent "shape parameter, κ" method

110   (Castle and Salvi, 2001a); *iii*) three Tougaard-like backgrounds: a) using the Tougaard universal

111   constants (Tougaard, 1988a and Tougaard, 1988b); b) the Seah specific element constants (Seah et

112   al., 2000); c) three parameters specific for the XPS analysis of transition metals proposed by

113   Tougaard (1997), respectively.

114

115   **EXPERIMENTAL**

116   XPS experiments were carried out with a Thermo VG THETA PROBE ESCA

117   spectrometer using monochromatic AlKα X-rays and an electrostatic hemispherical analyzer. The

118   spectra were recorded with pass energy of 100 eV, X-ray spot size of 400 μm, and step size of 0.1

119   eV. The base pressure in the analysis chamber was around 10^{-9} Torr or better. A flood gun was used

120   to correct for differential charging.

121   As reference standards for octahedral Ti^{4+} two types of TiO$_2$ samples and two natural

122   micas crystal were analyzed. The first type of oxide is a synthetic commercial TiO$_2$ powder (Carlo

123   Erba) with analytical grade; the other oxide is a natural crystal of brookite, which is one of five

124   polymorphs of titanium dioxide found in nature. Powder sample (synthetic TiO$_2$) was crushed under

125   acetone in order to prevent oxidation states changing in the sample. Both powder and brookite

126   sample were mounted onto an adhesive-coating copper tape. Care was taken to ensure that the

127   powder was uniformly dispersed onto copper tape, using a cleaned stainless-steel spatula so to

128   gently press the powder on the surface. During the XPS analysis it has been verified that no signals

129   from the tape itself (mainly composed of carbon, oxygen, silicon and copper) were detected.

130   Volcanic well characterized micas coming from S. Antonio Cave in Mt. Vulture (Potenza,

131   Italy), hereafter labelled SA (Schingaro et al., 2001), and from plutonic rocks (Black Hills,

132   Australia) (Schingaro et al., 2005), hereafter called BHG, were used to study the signal $2p$ of Ti and

133   Fe occurred in these kind of minerals. As known, their crystal structure is based on a complex unit

134   (layer) composed by an octahedral sheet (O) sandwiched between two tetrahedral sheets (T). These

135   layers are together essentially jointed by interlayer alkaline or alkaline earth cations. Micas can

136   crystalize in several polytypes (Scordari et al. 2012a; Scordari et al. 2012b; Mesto et al., 2012) with

137   symmetry ranging from trigonal to triclinic (Schingaro et al., 2013): the micas studied here belong

138   to monoclinic system, $1M$ polytype. In this polytype are present two symmetrically independent

139   octahedral sites, M1 and M2 and one tetrahedral site, T (Lacalamita et al., 2012).

140   SA mica was deeply investigated by Scordari et al. (2006) and Ventruti et al. (2009). In

141   this phlogopite, Fe and Ti have been accurately characterized by Mössbauer spectroscopy, crystal

142   structure and crystal chemistry investigations. Ti occurs in the structure only as Ti^{4+} in octahedral

143   coordination and in one site (M2), whereas Fe occupies both M1 and M2 sites, and occurs in two

144   oxidation states (Fe^{2+} and Fe^{3+}). SA phlogopite represents an ideal standard to study the Ti signal,

145   because this sample is very homogeneous in chemical composition and only one octahedral Ti^{4+}

146   species occurred. Unfortunately, analogous micas having only one Fe species in a single

147   crystallographic site has not been found so far by us. In spite of this, interesting results have been

148   obtained from the analysis of $Fe2p$ region for SA mica.

149   Plutonic mica, labelled BHG, was accurately investigated by Schingaro et al. (2005). The

150   structural formula was calculated using a combination of SCXRD, EPMA, Mössbauer and XPS

151   techniques, which yielded about 98% of Fe^{2+}/Fe_{tot} and Ti in multioxidation states, octahedrally

152   (Ti^{4+}, Ti^{3+}) and tetrahedrally coordinated (Ti^{4+}).

153   XPS investigation on mica samples have been carried out on a millimetric sized crystals,

154   exfoliated into the spectrometer degassing chamber, under N_2 atmosphere, to avoid interferences by

155   superficial contaminations or signal alterations by oxidation processes due to the exposition of the

156   sample surfaces to air. However, in spite of these precautions, a small amount of carbon was

157   detected during XPS measurements. This points out that the micas studied here are likely

158   characterized by an intrinsic adventitious carbon contamination.

159   Insulating samples (as most minerals), irradiated by X-ray tend to become positively

160   charged, thus shifting the peak positions. As common practice, carbonaceous surface contamination

161   was used to assess the extent of this shift. Therefore, for all the studied samples, the binding energy

162   (BE) scale was shifted so that the BE of the aliphatic component of C1s peak was at 284.8 eV.

163   Several methods have been used to evaluate the XPS spectrum background: Linear, Shirley

164   and Tougaard-like backgrounds have been processed by means of manufacturer's Avantage

165   software package v. 5.31, while "shape parameter, κ" background has been treated by means of

166   NEW-GOOGLY program (Castle et al, 2000), which was described in a previous work by Castle

167   and Salvi (2001a). Finally, the Levenberg-Marquardt algorithm (More, 1978) has been used for

168   performing non-linear least-squares curve fitting.

169   All spectrum features are fitted with a Voight function; no peak tail was used with the

170   "linear", "Shirley" and "shape parameter, κ" methods. Differently, when Tougaard background-

171   type was used, an exponential tail was added only to the fitted peaks of the main doublet

172   components. In all fits the components of the main doublets were constrained to the same

173   Gaussian/Loretzian (G/L) ratio, while satellite features (Salvi et al., 2004 and Langerame at al.,

174   2008) were considered as pure Gaussian peaks. For the 'Tougaard2parms", "Seah",

175   'Tougaard3parms" the B parameter was changed with respect to those quoted in bibliography, so

176   that the calculated background matched the signal in the highest binding energy region of the

177   spectrum. For the shape parameter, κ method the κ and B1 parameters were variables of the fitting

178   (see **Background removal method** section).

179

BACKGROUND REMOVAL METHODS

181   Two main and sensible parts of a XPS surface analysis are: subtracting of inelastic

182 background and fitting with a synthetic lineshape to the data. A serious problem in electron

183 spectroscopy is to isolate the part of a measured spectrum (which consists of inelastic-scattered

184 electrons) to determine the electron energy distribution at the point of excitation in the solid. The

185 problem was discussed by several authors (Repoux, 1992) and a number of methods have been

186 suggested (Aronniemi et al., 2005 and references therein). Still today, the correct background

187 removing from a XPS spectrum is not an easy task. It is known that part of the background source is

188 due to electrons photo-emitted from atoms (generally from inner layers) that during their travel

189 towards the surface experience a series of energy loss processes. As a consequence, their kinetic

190 energy is lower and contributes to the noise of the spectrum. The kinetic electron energy loss

191 processes can be ascribed to two main mechanisms: a) extrinsic losses, due to the electrons

192 traveling through the material by inelastic scattering events, b) intrinsic losses, associated with

193 photoelectron excitation of the electronic structure. The intrinsic losses do not change in proportion

194 to the main peak and can provide useful information for the full interpretation and quantification of

195 the XPS spectrum.

196   A critical analysis of this phenomenon was proposed by Tougaard (Tougaard, 1988a).

197 Although these two contributions to the background are probably inextricably mixed, Tougaard and

198 Sigmund (1982) and Tougaard (1988a) determined the approximate distribution of the extrinsic

199 losses from a priori principles with a fair success. However, because the intrinsic and extrinsic

200 contributions span similar energies, the value obtained for peak intensity strongly depends upon the

201 method used for the background subtraction. Some methods commonly used are:

202   *i) Linear background*: it is the first and simplest method used to subtract the background

203 from XPS spectrum, in which two arbitrary points are chosen, on either side of the peak of interest,

204 and joined by a straight line. This procedure can yield some reasonably success, with intense

205   narrow peaks and where intrinsic losses are not favoured, as for insulators having wide band gap,

206   (Sherwood, 1980) and leading to a peak with no intrinsic background step (and k equal to zero, see

207   next point: *v*). However, when peaks have broad widths, serious systematic errors can occur (Powell

208   and Seah, 1990).

209   *ii*) *Shirley background*: it is the wildest used background. This method assumes that the

210   inelastic scattered background has a delta function which is constant for all energy losses

211   (Sherwood, 1990). It is subtracted from the measured spectrum iteratively as:

212

$$F_{k+1}(E) = j(E) - j(E_{min}) \frac{\int_{E}^{E_{max}} F_k(T)dT}{\int_{E_{min}}^{E_{max}} F_k(T)dT} \qquad (1)$$

214   where j(E) is the measured energy spectrum intensity at kinetic energy E and $F_k(E)$ is the

215   background corrected spectrum after *k* interactions. Shirley's algorithm is usually used to determine

216   peak areas in a short energy window, thus subtracts a background that is mainly of intrinsic nature.

217   The relative intrinsic and extrinsic contributions depend on the integration limit (which are an

218   arbitrary choice) and on the electronic structure of the given atom in the given compound (Shirley,

219   1972). The use of this background is very pragmatig, leading always to a closed boundary to the

220   peak which can be easily integrated (Tougaard, 1988a). In particular, for insulator with a band gap

221   (as the micas studied here) and for some other materials, the Shirley background can exceed the real

222   background and leads to non-physical negative contribute to intensity. This causes systematic

223   uncertainties like those of linear background and it is universally recognised that the assumptions of

224   a Shirley background are difficult to justify (Salvi and Castle, 1998a). In particular systematic errors

225   can affect, very strongly, the results of the spectrum evaluation and this lack of accuracy is

226   particularly enhanced when the validity of the generated background has to be tested over large

227   energy separation from the main peak.

228   *iii) Tougaard background*: gives the best approximation of the extrinsic background due to

229   the extrinsic losses suffered by the electron in its travel through the solid, towards the detector. The

230   extrinsic background has no effect under the peak center but builds slowly from it and its correct

231   removal may then leave a peak with a step-like background made of intrinsic losses suffered by the

232   electron within the photo-excited atom was intensity depends on the given atom, its chemical state

233   and structure Tougaard (1988a). Tougaard has shown that for a homogeneous and infinite depth

234   distribution (i.e. bulk sample) the energy distribution of an electron escaping through the surface

235   F(E) can be calculated as:

236

237
$$F(E) = j(E) - \lambda_i \int_E^\infty j(E')K(E'-E)dE' \tag{2}$$

238

239   where λ_i is the inelastic electron mean free path and $K(E'- E)$ is the differential inelastic scattering

240   cross section (Tougaard, 1988a). For most metals and their oxide, the product j(E)K(E,T), where T

241   is the energy loss, is sufficiently similar and can be described by the Universal cross-section:

242

243
$$\lambda(E)K(E,T) \cong A(T) = \frac{BT}{(C+T^2)^2} \tag{3}$$

244

245   where B and C are parameters depending on material (Tougaard, 1988b).

246   However, for material with narrow plasmon structures the cross section in Eqn (3) cannot

247   be well described by a function with two parameters and a Three-parameter Universal cross section

248   should be used instead of Eqn (3) (Tougaard, 1997):

249

250
$$\lambda(E)K(E,T) = \frac{BT}{(C+T^2)^2+DT^2} \tag{4}$$

251

252   where B, C and D parameters are a function of the classes in which the solid are divided taking in

253   account the full width at half-maximum (FWHM) of the dominating peak shape of the inelastic

254   cross section. In the case of Fe and Ti, the following B, C and D parameters: 4210, 1000 and 13300,

255   have been respectively proposed (Tougaard, 1997).

256   *iv) Seah* background: it is possible define the Tougaard's C and B parameters as a function

257   of the centroid energy using the following equations background (Seah et al., 2000):

258
$$C = \left(\frac{2\overline{E}}{\pi} \right)^2 \qquad\qquad (5)$$

259

260
$$B = 2C \exp\left(-\frac{\overline{E}}{E_1} \right) \qquad\qquad (6)$$

261

262   where C is always an element-specific parameter and B must be adjusted in fitting to take into

263   account the depth profile element distribution.

264   The strength of Tougaard-like backgrounds is that it is independent from arbitrary user

265   choose on the endpoint selection, it make use of a solid theory, but on the other hand, the acquired

266   spectrum must be wide enough so that the correct value of B can be determined.

267   *v) Shape paramter, κ*: more recently, Castle and Salvi (2001a) proposed a modification of

268   Shirley background where the $J(E_{min})$ is referred to a shape parameter, κ, and the integration

269   function is multiplied with a first order polynomial. The *k*-shape parameter method fits the whole

270   spectra by merging the intrinsic part defined by k-costant using a Shirley-type routine in a

271   consistent manner with a polynomial tail intended to retrace the Tougaard's extrinsinc background

272   associate to each peak (Salvi and Castle, 1998 a and b). When the tail is extrapolated back to energy

273   defining the midpoint of the peak, the intercept normalized by division by peak area gives a

274   parameter, called "shape parameter, κ" which defines the step-like peak shape. The polynomial tail

275   is expressed in the following equation:

276

277
$$P = \kappa + B1(E-E_0) + B2(E-E_0)^2 \qquad\qquad (7)$$

278

279   where E_0 is the peak centre energy, $E-E_0$ expresses the distance in electron volt from the peak

280   center, B2 is usually set to zero so the equation (7) approximated the peak tail as a straight-line. κ

281   and B1 express the step-like peak proportionality and background slope, respectively, which are

282   fitting variables in the background evaluation procedure. The idea is to retain, on routinely bases,

283   the advantage of using the set of semi-empirical sensitivity factor derived by Wagner (Sherwood,

284   1990) for the peak areas normalization. Moreover for near-peak spectral windows and 'clean'

285   sample with flat extrinsic tail (as in this paper), the first order polynomial is fairly matching the

286   Tougaard background slope outside the peak region. The κ parameter is a good indicator of the

287   intrinsic component of the peak; it is independent of the presence of overlayer on sample and of

288   instrumental factor (such as pass energy and X-ray source). Castle and Salvi (2001b) demonstrated

289   that κ increases toward midpoint of d series (especially for 3d series) and reflects the rise to a

290   maximum in the number of final state configuration available as a result of photoelectron process. It

291   can give information on the bond character in compound and alloys and provides a more reliable

292   basis for treatment of the background during peak fitting (Castle and Salvi, 2001a). Instead, B1

293   parameter acts as an in-depth indicator, where an increase in background slope after the peak points

294   to a composition gradient decreasing towards the surface and vice versa (Castle and Salvi, 2001b).

295   In this work for the first time the "shape parameter, κ" has been applied to the study of

296   natural mica samples (phlogopites) and titanium oxide (brookite).

297

298   **RESULTS**

299   **C1s and O1s spectra**

300   Fig. 1a and 2a shows, respectively, XPS spectrum of C*1s* and O*1s* region for a brookite

301   single crystal, after that the background was subtracted according to Shirley method. Both spectra

302   can be deconvoluted by three components. C1s features (FWHM = 1.7 eV) can be assigned to

303   aliphatic, alcholic and ketonic carbon, while the two major components of O1s level (FWHM =

304 1.32 eV) can be ascribed to oxyde and hydroxyl oxygen atoms. In addition, a minor amount of

305 water, likely adsorbed on the mineral surface, was also found.

306 The fitting of C1s and O1s peak for SA single crystal mica is shown in Fig 1b and 2b,

307 respectively. Similarly to brookite specimen, the backgrounds were treated as suggested by Shirley.

308 The C1s signal can be fitted by three components, but they are narrower (FWHM = 1.4 eV)

309 compared to brookite case. Differently, only two features (O^{2-} and OH^{-}) wider (FWHM = 2.0 eV)

310 than the ones of brookite, contribute to the envelope of O1s signal. Their binding energies are

311 comparable with the ones of silicate minerals (Schingaro et al., 2004). Similar results have also

312 been found for BHG mica (Fig 1c and 2c).

313 The O1s lineshape broadening for the mica samples seems not be caused by the sample

314 charging problem, as proved by the opposite trend found for the widths of C1s and O1s signals, in

315 brookite and mica sample.

316

Ti2p spectra

318 Fig. 3 shows the Ti2p region of the acquired Ti^{4+} reference synthetic powder sample after

319 the background has been evaluated using six different methods, referred to as "Linear", "Shirley",

320 ''Tougaard2Parms'', "Seah", 'Tougaard3Parms'' and ''Shape parameter, κ''. The spectrum

321 features consist in the main 2$p_{3/2}$ and 2$p_{1/2}$ doublet and several satellite peaks that are typical for

322 Ti2p signal (Moretti et al. 2004; Moslemzadeh et al., 2006; Langerame et al. 2008). The

323 background slope of this region is quite flat as expected on relatively clean samples (Castle, 2002).

324 For the Linear and Shirley background, the parameters to be defined are the endpoints of

325 the background curve. Here the start point was set at the low binding energy side of the 2$p_{3/2}$ peak

326 (454 eV) and the end point to the local intensity minimum at the high binding energy side of the

327 main Ti2p doublet present in the spectrum (467 eV).

328 In the case of ''Tougaard2parms'', "Seah", 'Tougaard3parms'' and κ, shape parameter the

329 background was calculated using the energy range 452–500 eV. The final values of the parameters

330   used for each fitting have been reported in Fig 3. The most important spectral parameters obtained

331   as the result of the fitting are presented in Table 1. It is observed that all backgrounds give similar

332   values for the number of components, full width at half maximum (FHWM) and binding energy

333   (BE) peak position. Some changings are instead found for the ratio of the $2p_{3/2} - 2p_{1/2}$ intensity. The

334   theoretical ratio expected between the main components for a $2p$ doublet is 0.52 (Scofield, 1976),

335   thus the values obtained here is too low for Tougaard-like methods (2 and 3parms) and contrarily

336   high for linear type-background (Table 1). If, however, the broadening was constrained to the

337   Scofield value, the resulting curve fitting were again good. Actually the following chi-square values

338   were obtained: 5.01 for "linear", 1.65 for "Shirley", 2.63 for ''Tougaard2parms'', 5.24 for ''Seah'',

339   3.66 for ''Tougaard3parms''and 1.40 for "shape parameter, κ".

340   The underestimate of $2p_{1/2} - 2p_{3/2}$ intensity ratio found in the Tougaard-like background

341   can be justified invoking the decreased lifetime of the $2p_{3/2}$ hole caused by the Coster–Kronig

342   process (Nyholm et al., 1981) that can result in a peak broadening. But it has been observed that the

343   peak line-widths for all backgrounds result to be comparable; therefore, in this specific case, it

344   seems to be more likely that Tougaard-like backgrounds eliminate too much intensity from $2p_{1/2}$

345   component.

346   Differently the "Linear" method seems to remove a bit much intensity from $2p_{3/2}$, the

347   chosen of the end point strongly affects the peak intensity for this background. Indeed, even when

348   high BE region is considered in the fitting (background limits from 458 eV to 480 eV) the $2p_{1/2}$-

349   $2p_{3/2}$ intensity ratio drastically increases, reaching a value equal to 0.69.

350   Finally, "Tougaard2parms", "Tougaard3parms" and "κ, shape parameter", compared to

351   "Seah" background have shown a propensity to overemphasizing the influence of surface excitation

352   as proved from satellite relative intensity. The specific Three-parameters universal cross section for

353   Ti, Fe and other transition-metal was developed by Tougaard to the purpose to minimize the

354   characteristic of previous universal cross-section, but as stated by the same author it is found no

355   clear evidence that the Three-parameters cross section is more accurate than the Universal cross-

356   section (Tougaard, 1997).

357   The Ti2p spectrum acquired by a brookite crystal is represented in Fig. 4. The

358   characteristics of the spectrum are very similar to those in the photoelectron powder spectrum. It is

359   possible distinguishing the main doublet and a number of satellite peaks. The highest BE satellite

360   peak has a bigger intensity and is located at higher BE value with respect to that of TiO$_2$ powder

361   (Table 1). This characteristic seems to be related with the measurements carried out on single

362   crystal. As a matter of fact, the same shift and intensity increment is found in the XPS spectra of

363   mica samples (see below). Ti2p background of brookite crystal has a trend like that of powder

364   sample, that is a flat slope and with a typical background-like step (see the κ and B1 values of the κ;

365   shape parameter method in Fig. 4).

366   The same BE ranges of the "linear" and "Shirley" backgrounds as used for TiO$_2$ powder,

367   have been applied to the brookite Ti2p region, while the remaining background removal methods

368   were processed with 450.0-510.7 eV BE range. All methods used for the removing of background

369   result in an expected single Ti species with a BE shifted to about 0.5 lower value as to that of the

370   Ti2p signal of TiO$_2$ powder reference. The component FWHM of the main doublet is close to the

371   line width of TiO$_2$ powder. Both "Linear" and "Shirley" overestimate Ti2$p_{1/2}$/Ti2$p_{3/2}$ ratio, whereas

372   "Tougaard2parm", "Seah" and "Tougaard3parm" underestimate it. Similar consideration

373   concerning the effects of the background subtraction experienced in the powder sample can be

374   extended to the brookite single crystal.

375   In Fig. 5a, 5b (SA) and 6a, 6b (BHG) the best curve fitting of the Ti2p and Fe2p region

376   are reported, while the main parameters obtained by the fitting have been reported in Table 2 and 3.

377   The removing of the background has been performed in the same way of the reference oxide spectra

378   for SA phlogopite. For BHG spectra only the "shape parameter, κ"-like background has been

379   evaluated. The values of the B, C and D parameters used for Tougaard-like backgrounds and κ and

380   B1 refined for the "shape parameter, κ" method are reported inside the figures.

381   XPS spectra of the Ti2p regions of SA and BHG samples (Fig. 5a and 6a) are similar to the

382   Ti signal of reference oxide spectra, but in the case of the micas, the intensities of the high BE

383   satellite peaks close to the main doublet are lower compared with the same signals of TiO$_2$ powder

384   and Brookite. The highest satellites have position and intensity very close to the highest ones in the

385   brookite spectrum (Table 1 and 2). The start and end BE points for the "linear" and "Shirley"

386   background has been set to 454.0 and 468.0 eV respectively, while the remaining background

387   removing methods were carried out with a 454.0-510.0 eV BE range.

388   The components of the main doublet in these regions have a FWHM significantly broader

389   than line-widths found in both TiO$_2$ powder and brookite sample. The broadening of the signal

390   seems do not be a consequence of the sample charging or instrumental problem, as shown by an

391   internal check on linewidth values of C1s signal. Every attempt of fitting the Ti2p doublet of the SA

392   phlogopite using features with line-width comparable to ones of the TiO$_2$ reference spectra results

393   in a multi-component fitting, dividing out part of Ti^{4+} and all Ti^{3+} in octahedral coordination, and

394   part of Ti^{4+} in tetrahedral site. This contrasts with the Ti speciation obtained for the SA sample by

395   the converging result of several techniques such as X-ray diffraction, EPM analysis, SIM

396   spectrometry, Mössbauer spectroscopy and neutron diffraction (Scordari et al. 2006; Ventruti et al.

397   2009).

398   When no restrain is imposed on line width, all background removing methods yield to only

399   one Ti species both for SA and BHG micas with a BE close to that found in the TiO$_2$ powder

400   reference spectrum.Fig. 5a and 6a show that the background slope for the Ti2p regions has a

401   negative trend and the satellite peaks close to the main peak are almost overcrowded from the

402   spectrum noise. These singularities are very unusual for Ti2p signal, but generally these background

403   slopes are typical of Fe2p region (Castle et al., 2001c).

404   Even if we used a range from 700.0 eV to 775.0 eV for the calculation of background-like

405   Tougaard it was not possible find suitable B, C and D parameters which reproduced the background

406   trend distant from the main doublet. Therefore, a background which matched the acquired spectra at

407   about 20 eV from the 3/2 component of the signal have been used. The chosen parameters lead to

408   an underestimate of the peak at $\approx$ 38 eV from the main peak.

409   The main parameters resulting from the curve fitting of Ti2p region for SA and BHG

410   samples are reported in Table 2 and 3. Satellite peaks have been fitted as pure Gaussian peaks,

411   whereas an exponential tail was added to the remaining curve fitted features, as for the case of

412   reference oxides.

413   For SA mica, when no restrain was imposed on the ratio of the peak areas of 2$p_{1/2}$-2$p_{3/2}$

414   components, it has been observed that all methods for the background treatment yielded very

415   similar values in terms of line widths. Apart "Tougaard3parm", they give acceptable values for the

416   Ti2$p_{1/2}$-Ti2$p_{3/2}$ intensity ratio. The following ratios have been obtained: 0.48 (χ^2=0.11) for "Linear",

417   0.52 (χ^2=0.12) for "Shirley", 0.52 (χ^2=2.47) for "Tougaard2parm", 0.48 (χ^2=1.69) for "Seah", 0.45

418   (χ^2=1.80) for "Tougaard3parm" and 0.50 (χ^2= 0.12) for "shape parameter, κ". The "Linear" and

419   "Shirley" method have a χ^2 lower with the respect to the ones of other methods because these

420   methods are processed in a shorter BE window than the other ones. Regarding the Tougaard-like

421   background, the "Tougaard2parm" method yielded the expected value for the ratio between the

422   main component of the Ti2p doublet but it have also the highest χ^2, therefore it reproduce with less

423   efficiency the experimental spectrum. Among the Tougaard-like background methods, the lowest χ^2

424   has been obtained with the parameters of "Seah" (χ^2 = 1.69), but it result in a value of 0.48 as ratio

425   between 2$p_{1/2}$-2$p_{3/2}$ components. If the theoretical ratio is imposed to the peak areas (see Table 2)

426   the χ^2 rise to 1.71, which shown that the fitting is again good. "Tougaard3parm" results in an

427   underestimate of the Ti2$p_{1/2}$ component, but if the peak areas are constrained to the expected value

428   the χ^2 rise from 1.80 to 2.20.

429   Finally, the "shape parameter, κ" method results in a κ value of 0.031 and a B1 parameter

430   of -0.00012 which proves the slightly negative background slope in the higher BE region. The value

431   of the κ parameter for the SA mica is lower than the κ values found for the reference spectra and

432   those reported in literature for TiO_2 oxides (Castle and Salvi, 2001b).

433   Similar results have been obtained for BHG sample (Table 3). FHMWs of Ti2p doublet

434   are very close to values of SA mica pointing out that, in contrast to Schingaro et al., 2005, only

435   octahedral Ti^{4+} occurs in BHG phlogopites. In particular, the evaluation of Ti2p signal by means of

436   the shape parameter, κ, background removing procedure results in a κ value of 0.024 and B1 -

437   0.0004 (Fig. 6a), which are close to that found for SA crystal.

438

439   **Fe2p spectra**

440   Fig. 5b and 6b represent the Fe2p signals for mica samples elaborated using the same

441   criteria of Ti2p region for the background evaluation. The BE range used for the "linear" and

442   "Shirley" background starts from 705.0 eV and ends to 733.0 eV. The other backgrounds were

443   carried from 705.0 to 775.0 eV BE range.

444   Since we have not either any reference compounds for the Fe2p signal in mica and

445   considering that the Fe(II) and Fe(III) are in high-spin states, we have adapted the fitting strategy

446   proposed by Grosvenor et al, 2004, for the 3/2 component of the Fe2p signal, processing both Fe2p

447   component. The minor number of fitting parameters and constrains was used in the fitting as

448   possible.

449   The final parameter of the multiplet used to deconvolve the Fe2p signal of SA mica are

450   reported in Table 2. For the Fe2p signal of the SA sample, the Tougaard like backgrounds

451   emphasized the superficial excitation, leading to the higher intensity for the satelite peaks (Fig 5b).

452   Interesting information has been provided by the analysis of the background with the

453   "shape parameter, κ" method, not obtained by the other ones. For SA mica, the κ method results in

454   a B1 value of -0.0007 which describes the negative slope of the background similar to the slope

455   found for the Ti2p region. The κ value obtained from the fitting is 0.077, which is sensibly lower if

456   compared with the expected one in the ferric oxides (0.095) (Castle and Salvi, 2001a). This value is

457   close to the κ parameter of the Ti2p region (i.e. 0.049 for TiO_2 oxide). Finally in the region of the

458   Fe2p some satellite peaks are present, these are unusual for the Fe2p signal but common for the

459   Ti2p signal (Salvi and Castle, 1998b). A similar behaviour has been reported for Fe2p signal in iron

460   silicide were in the presence of weak satellite peaks and a very low κ value was associated if

461   compared to elemental and oxide iron (Castle et al., 2001c). This information could suggest that an

462   orbital screening effect between Ti and Fe occurs in mica crystals. On the light of this result an

463   analysis of Fe2p signal of BHG sample, evaluating the background by means of the only shape

464   parameter, κ method, was carried out (Table 3). It yielded analogous results to the ones obtained for

465   SA mica. The BHG Fe2p signal has a $\kappa = 0.058$ significantly lower than that of iron oxides, similar

466   to SA crystal. The final fitted value of B1 parameter was -0.0007, proving the unusual negative

467   slope for this background. Finally, some satellite peaks have been found at high BE (Fig 6b), which

468   are more intense than the ones of SA.

469   As concerns the quantitative Fe speciation, the results of the Fe^{2+}/Fe_{tot} proportion for SA

470   phlogopites are about 47 % for "Linear", 55 % for "Shirley", 55 % for "Tougaard2parm", 53 % for

471   "Seah", 55 % for "Tougaard3parm" and 53% for "shape parameter, κ". With the exception of

472   "Linear" method, all background method yielded to a value for Fe^{2+} comparable to the expected one

473   (57%) as derived from Mössbauer investigations (Scordari et $al.$, 2006). Differently, Fe quantitative

474   analysis for BHG sample yielded in 65 % of Fe^{2+}/Fe_{tot} ("shape parameter, κ") clearly

475   underestimated if compared to Mössbauer data, $Fe^{2+} \approx 98\%$ (Schingaro et al. 2005). The reason of

476   the underestimation, maybe, is a consequence of a stronger dependence of the Fe2p lineshape of

477   BHG by Ti-Fe screening effects (See below: **DISCUSSION section**).

478

479   **DISCUSSION**

480   Mica crystals of the sample SA have been deeply investigated in the past by Schingaro et

481   al., 2001 and Ventruti et al., 2009. According to these studies, the cation distribution of Ti end Fe in

482   SA crystals is well-know: Ti, as Ti^{4+}, is at M2, whereas Fe, as Fe^{2+} and Fe^{3+}, fill M1 and M2 site in

483   the ratio 57:43.

484   The cation distribution in BHG Ti-rich phlogopites was proposed by Schingaro et al.

485   (2005). Ti partitioning was calculated on the basis of XPS analysis, using the Shirley background.

486   The Ti2p photopeak was deconvoluted using components with FHMW comparable to the line width

487   of TiO_2 XPS powder spectrum acquired. The XPS result was: Ti^{3+} octahedral (26%) and Ti^{4+} at

488   octahedral (60%) and tetrahedral (14%), respectively, while Fe speciation, carried out by

489   Mössbauer investigation, yielded $Fe^{2+}/Fe^{3+} \approx 30$.

490   The curve fitting based on TiO_2 FHMW values yielded more than one Ti species for SA

491   sample in contrast with recent results, see: Scordari et al. (2006) and Ventruti et al. (2009).

492   Therefore for both mica samples, checked the absence of any sample charging, we conclude that the

493   TiO_2 narrow FWHMs cannot be used as reference values for the fitting, because they wrongly

494   represent the intrinsic characteristic of mica Ti2p signal having significant broad peaks. This result

495   is in agreement with Nesbitt et al., 2004. Borr (1993) ascribed the line width of non-conductive

496   samples to severe differential charging of surface. In the attempt to minimize differential charge

497   broadening, several kind of electron flood guns have been employed (Cazoux, 1999). However,

498   even when non-charge broadened thin films of Al_2O_3 and SiO_2 grown on Al (Berg et al., 1993) or Si

499   (Himpsel et al, 1998) have been investigated, the 2p core-level widths continued to be significantly

500   great, proving that, as for the mica here investigated, charge-broadening does not give an

501   appreciable contribute to FWHM of the photopeak when an flood-gun is properly used with

502   spectrometers equipped with modern monochromated Alkα source.

503   Nesbitt et al, 2004, have shown that the primary control of FWHM of Si2p in olivine, SiO_2

504   and eventually other silicates is vibrational broadening. With the ejection of a photoelectron, the

505   atom assumes an electronic excited state (contains an "electronic hole" in a core orbital). Various

506   vibrational quantum level of the excited electronic state can be accessed upon photoemission

507   (Karlesen et al., 2001, and Nesbitt et al., 2004 and reference therein). Each vibrational level is

508   energetically distinct and has a specific binding energy associated with the process of

509   photoemission. This implies that the XPS spectrum of such core line include the entire suite of these

510   vibrational final state peaks and if a large number of vibrational states is accessible during the

511   photoemission, the resulting spectra envelope of the core line (i.e. Ti2p level) is invariably broad,

512   depending on inherent line width of vibrational states, number of contributing to the envelope and

513   on the energy separating each final-state peak.

514   Moreover, 2p core line shape of transition metal can also be affected by the screening

515   effect when other transition metal ions are occurred, as for the case of the mica here investigated.

516   Fuggle et al. (1980) has shown as the understating of the core-level screening mechanism is crucial

517   in core-level spectroscopies and in particular for the XPS technique. The line-shapes of core level

518   peaks in XPS depend critically on the coupling of the screening level to the other (delocalized)

519   occupied levels of the initial state. The authors observed that the line shapes of core level of Ti, Th

520   and Ce elements and some of their intermetallic compounds and lanthanide oxides are directly

521   related to the degree of localization of screening orbitals. Similar results have been obtained by Van

522   Veenendoal and Sauotzky (1993), which have investigated the peak shape of Ni2p signal. These

523   authors have demonstrated as the occurrence of transition metal can severely influence the peak

524   shape of the 2p photoelectron spectra. This effect is due to the competition between screening

525   electron coming from the surrounding ligands and electron coming from ligands around a

526   neighboring transition metal ion. It depends strongly on the nature of the surrounding atoms and

527   also on their valence.

528   From the above discussion, it is apparent that the choice of a reference compounds for XPS

529   investigation should be performed with extreme care. The crystal structure of the standard should be

530   as similar as possible to the compounds which have to be investigated, so that is possible to take in

531   account the matrix effect broadening on the XPS signal. In this work, for the first time, a well and

532   full-characterized mica (SA) is used as standard for the Ti^{4+} in octahedral site, moreover even if Fe

533   in SA mica occurs with more than one oxidation state, nevertheless the results of the Fe2p fitting

534   can be extended to other micas with different crystal chemistry.

535   Taking into account the new information provided from the background analysis by means

536   of the shape parameter, κ, a screening effect between Ti and Fe (Platonov et al.,1991; Sherman,

537   1987; Seda and Herne, 2004) in the mica could be argued. This phenomenon likely is more apparent

538   for BHG mica. However, this effect deserves to be supported by more thorough studies, which can

539   be the subject of forthcoming publications.

540

541   **FINAL COMMENT**

542   XPS spectra of 2p region of Ti and Fe in natural minerals, such as micas, are complex and

543   rich of features (asymmetric peaks, shake-up satellites, strong intrinsic background, etc.). From this

544   point of view XPS background represents an important source of information, which can provide

545   further knowledge about the transition metal speciation and their distribution, when a suitable base

546   for the interpretation of XPS signals is employed.

547   In the case of the ratio Fe^{2+}/Fe^{3+} derived from the relative peak area values the effect of the

548   background choice has been observed resulting in a fluctuation of about 10% unit. By the

549   comparison of the curve fitting carried out on TiO_2 oxide systems and mica sample is resulted that

550   the use of suitable standard which can reproduce the matrix effects on the peak broad is an essential

551   step. Extreme care should be used during the choice of reference compounds in order to get

552   accurate results from XPS investigation. XPS analysis on TiO_2 synthetic powder and natural

553   brookite single crystal indicate that they give the same FHWM and that such compounds are not

554   appropriate standard for Ti2p signal in complex silicate matrix, i. e. natural micas. In this paper, a

555   full and well characterized natural mica crystal, coming from Mt. Vulture (Italy) and named SA, has

556   been used as reference for Ti2p signal in these classes of compound. As a matter of fact, the

557   multicomponent fitting of Ti2p signal proposed for BHG sample by Schingaro et al., 2005, is in

558   contrast with the results of this paper. The crystal formula proposed by the same authors should be

559   revised; in fact the FHMW of Ti2p signal of this sample is close to one of standard SA phlogopites,

560   pointing out that only octahedral Ti^{4+} occurs in BHG mica.

561   Finally, for the first time the "Shape parameter, κ" background was applied to the study of

562   mica mineral phase. In general, the comparison between Shirley and Tougaard background shows

563   the latter to be better (Jansson et al., 1995), but for the studied cases, all the used Tougaard-type

564   backgrounds, have shown to be not able to reproduce the background trend of experimental

565   spectrum for Ti2p region.

566   This behavior cannot be ascribed to the superficial contamination of samples which results

567   to be negligible as proven by the spectra background slopes, maybe it is be due to the low intensity

568   of the collected signals. Differently, the "Shape parameter, κ" method for background removing has

569   shown to be not so sensible to the signal intensity providing a plausible background for all the

570   spectra investigated. It leads to similar results to common Shirley background as concerns the

571   speciation of transition elements, but in addition, can provide supplementary information by the

572   study of spectrum background. . In addition, XPS results are in agreement with the cation

573   distribution for SA micas proposed by Ventruti et al. (2009)

574   Finally, we think that the useful comparison here performed on single crystal and "clean"

575   sample should be necessary continued by taking in consideration more complex spectra in order to

576   both further judge the performance and the limits (mainly computational) of each background

577   removal methods and to investigate the occurrences of charge transfer process in other

578   phyllosilicates.

579

584

585

References cited

587 Aronniemi, M, Sainio, J., Lahtinen, L. (2005) Chemical state quantification of iron and chromium

588   oxides using XPS: the effect of the background subtraction method. Surface Science 578,108-

589   123. DOI:10.1016/j.susc.2005.01.019.

590 Berg, C., Raaen, S., Borg, A., Andersen, J. N., Lundgren, E., Nyholm, R. (1993) Observation of a

591   low-binding-energy peak in the 2p core-level photoemission from oxidized Al(111). Physical

592   Review B, 47 (19), 13063-13066. DOI: 10.1103/PhysRevB.47.13063.

593 Borr, T. (1993) Modern ESCA, the principles and Practice of X-ray Photoelectron Spectroscopy.

594   CRC press, Boco Raton, Florida.

595 Castle, J.E. (2002) A wizard source of expertise in XPS. Surface and Interface Analysis, 33, 196-

596   202. DOI: 10.1002/sia.1202.

597 Castle, J.E., Chapman-Kpodo, H., Proctor, A.and Salvi A.M. (2000) Curve-fitting in XPS using

598   extrinsic and intrinsic background structure. Journal Electron Spectroscopy and Related

599   Phenomena, 106/1, 65-80.

600 Castle, J.E.and Salvi, A.M. (2001a) Chemical state information from the near-peak region of the X-

601   ray photoelectron background. Journal of Electron Spectroscopy and Related Phenomena, 114-

602   116, 1103. DOI: 10.1016/S0368-2048(00)00305-4.

603 Castle, J.E. and Salvi, A.M. (2001b) Characterisation and Use of Intrinsic Background in XPS.

604   Analytical Sciences 17, i147-i150.

605 Castle, J.E., Salvi, A.M. and Guascito, M.R. (2001c) Analysis of the x-ray photoelectron energy-

606   loss background in silicides. Surface and Interface Analysis, 31, 881-889. DOI:

607   10.1002/sia.1124.

608 Cazoux, J.(1999) Mechanisms of charging in electron spectroscopy. Journal of Electron

609   Spectroscopy and Related Phenomena, 105, 155-185. DOI: 10.1016/S0368-2048(99)00068-7

610   Cesare, B., Cruciani, G., and Russo, U. (2003) Hydrogen deficiency in Ti-rich biotite from anatectic

611   metapelites (El Joyazo, SE Spain): Crystal-chemical aspects and implications for high-

612   temperature petrogenesis. American Mineralogist, 88, 583-595.

613   Dyar, D.M. (2002) Optical and Mössbauer spectroscopy of iron micas in Reviews in Mineralogy

614   and Geochemistry. Edite by. Mottana, A., Sassi, F.P., Thompson, J.B. Jr., and

615   Guggenheim, S. vol. 46, 313-350. ISBN 0-939950-58-8.

616   Fuggle, J.C., Campagna, M., Zolmierek, Z., Lässer, R. and Platou, A. (1980) Observation of a

617   Relationship between Core-Level Line Shapes in Photoelectron Spectroscopy and the

618   Localization of Screening Orbitals. Physical Review Letters, 45(19), 1597-1600. DOI:

619   10.1103/PhysRevLett.45.1597.

620   Ghosh, T.B. and Sreemany, M. (1993) On the selection of an integration limit for quantitative XPS

621   analysis. Applied Surface Science, 64(1), 59–70. DOI: 10.1016/0169-4332(93)90021-3.

622   Grosvenor, A. P., Kobe, B. A., Biesinger, M. C. and McIntyre, N. S. (2004) Investigation of

623   multiplet splitting of Fe 2p XPS spectra and bonding in iron compounds, Surface and Interface

624   Analysis, 36, 1564-1574.

625   Hawthorne, F.C. (1988) Mössbauer Spectroscopy. In Hawthorne F. C. (Eds.) Spectroscopic

626   method in Mineralogy and Geology. Reviews in Mineralalogy., vol. 18, pp. 255-340.

627   Mineralogiacl Society of America, Chantilly, USA.

628   Henry, D.J. and Guidotti, C. (2002) Titanium in biotite from metapelitic rocks: Temperature effects,

629   crystal-chemical controls, and petrologic applications. American Mineralogist, 87, 375-382.

630   Henry, D.J., Guidotti, C., Thomson, J.A. (2005) The Ti-saturation surface for low-to-medium

631   pressure metapelitic biotites: Implications for geothermometry and Ti-substitution mechanisms.

632   American Mineralogist, 90, 316-328. DOI: 10.2138/am.2005.1498.

633   Himpsel, F.J., McFeely, F.R., Taleb-Ibrahim, A. and Yormoff, J.A. (1998) Microscopic structure

634   of the SiO_2/Si interface. Physical Review B, 38, 6084-6096. DOI: 10.1103/PhysRevB.38.6084.

635   Jansson, C., Tougaard, S., Beamson, G., Briggs, D., Davies, S. F., Rossi, A., Hauert, R., Hobi, G.,

636   Brown, N. M. D., Meenan, B. J., Anderson, C. A., Repoux, M., Malitesta, C., Sabbatini, L.

637   (1995) Intercomparison of algorithms for background correction in XPS. Surface Interface

638   Analysis, 23, 484. DOI: 10.1002/sia.740230708.

639   Karlesen, T., Sathe, L.J., Borve, K.J., Berreh, N., Kukk, E., Bozek, J.D., Coroll, T.X. and Thomas,

640   T.D. (2001) Vibrational Structure and Vibronic Coupling in the Carbon 1s Photoelectron

641   Spectra of Ethane and Deuteroethane. Journal of Physical Chemistry A, 105, 7700-7706

642   Kühberger, A., Fehr, T., Huckenholz, H. G., Amthauer, G. (1989) Crystal chemistry of a natural

643   schorlomite and Ti-andradites synthetised at different oxygen fugacity. Physics and Chemistry of

644   Minerals, 16, 734-740. DOI: 10.1007/BF00209694.

645   Lacalamita, M., Mesto E., Scordari, F. and Schingaro, E. (2012). Chemical and structural study of

646      $1M$- and $2M_1$-phlogopites coexisting in the same Kasenyi kamafugitic rock (SW Uganda).

647   Physics and Chemistry of minerals, 39, 601-611. DOI: 10.1007/s00269-012-0515-y

648   Langerame, F., Salvi, A.M., Silletti, M., Moretti, G. (2008) XPS characterization of a synthetic Ti-

649   containing MFI zeolite framework: the titanosilicalites-TS-1. Surface and Interface Analysis

650   40(3-4), 695-699.

651   Malitesta, C., Losito, I., Scordari, F. and Schingaro, E. (1995) XPS investigation of titanium in

652   melanites from Monte Vulture (Italy). Europena Journal of Mineralogy, 7, 847-858.

653   Marabini, A.M., Contini, G. And Cozza, C. (1993). Surface spectroscopic techniques applied to the

654   study of mineral processing. International Journal of Mineral Processing, 38,1-20. DOI:

655   10.1016/0301-7516(93)90062.

656   Mesto, E., Scordari, F., Lacalamita, M. and Schingaro, E. (2012). Tobelite and NH_4^+-rich muscovite

657   single crystals from Ordovician Armorican sandstones (Brittany, France): Structure and crystal

658   chemistry. American mineralogist, 97, 1460-1468. DOI: 10.2138/am.2012.4023

659   More, J. (1978) The Levenberg-Marquardt algorithm: Implementation and theory. Lecture Notes in

660   Mathematics, 630, 105-116. DOI: 10.1007/BFb0067700.

661   Moretti, G., Salvi. A.M., Guascito, M. R., Langerame, F. (2004) An XPS study of Microporous and

662   Mesoporous Titanosilicates. Surface and Interface Analysis, 36, 1402-1412.

663   Moslemzadeh, N., Beamsonb, G., Tsakiropoulos, P., Watts, J.F., Haines, S.R., Weightman, P.

664   (2006) Electronic structure of Ti metal and TiO2 powder studied by hard and soft (Cu Kα_1 and

665   Al Kα_1) X-ray photoelectron and Auger spectroscopy. Journal of Electron Spectroscopy and

666   Related Phenomena, 152, 148–151. DOI: 10.1016/j.elspec.2006.05.003.

667   Nesbitt, H.W., Bancroft, G.M., Davison, R., McIntyre, N.S. and Pratt, A.R. (2004) Minimum XPS

668   core-level line widths of insulators, including silicate minerals. American Mineralogist, 89, 878-

669   882.

670   Nyholm, R., Martensson, N., Lebugle, A., Axelsson, U. (1981) Auger and Coster-Kronig

671   broadening effects in the 2p and 3p photoelectron spectra from the metals ^{22}Ti-^{30}Zn. Journal of

672   Physics F: Metal Physics, 11, 1727-1733.

673   Platonov, A.N, Langer, K., Matsuk, S.S., Taran, M.N., and Hu, Y. (1991) Fe (super 2+) -Ti (super

674   4+) charge-transfer in a garnets from mantle eclogites . European Journal of Mineralogy, 3, 19-

675   26.

676   Powell, C.J. and Seah, M. P. (1990) Precision, accuracy, and uncertainty in quantitative surface

677   analyses by Auger-electron spectroscopy and x-ray photoelectron spectroscopy. Journal of

678   Vacuum Science & Technology A: Vacuum, Surfaces, and Films, 8 (2), 735-763. DOI:

679   10.1116/1.576956.

680   Rager, H., Geiger, C.A., Stalh, A. (2003) Ti(III) in Msynthetic pyrope A single-crystal electron

681   paramagnetic resonance study. European Journal of Mineralogy, 15, 697-699. DOI: 10.1127/

682   0935-1221/2003/0015-0697

683   Repoux, M. (1992) Comparison of background removal methods for XPS. Surface and Interface

684   Analysis, 18 (7), 567–570. DOI: 10.1002/sia.740180719

685   Salvi, A.M. and Castle, J. E. (1998a) The intrinsic asymmetry of photoelectron peaks: dependence

686   on chemical state and role in curve fitting. Journal of Electron Spectroscopy and Related

687   Phenomena , 95, 45-56. DOI: 10.1016/S0368-2048(98)00205-9.

688   Salvi, A.M., Castle, J. E. (1998b) The intrinsic asymmetry component of the "total background" in

689   XP spectra. Journal of Electron Spectroscopy and Related Phenomena, 94, 73-87. DOI:

690   10.1016/S0368-2048(98)00083-8.

691   Salvi. A.M., Guascito, R.M., Langerame, F. (2004) An XPS study of Microporous and Mesoporous

692   Titanosilicates. Surface and Inetrface Analysis, 36, 1402-1412.

693   Schingaro, E., Scordari, F., and Ventruti, G. (2001) Trioctahedral micas-1*M* from Mt. Vulture

694   (Italy): Structural disorder and crystal chemistry. Eur. J. Mineral., 13, 1057-1069. DOI:

695   10.1127/0935-1221/2001/0013-1057.

696   Schingaro, E., Scordari, F., Pedrazzi, G., and Malitesta, C., (2004) Ti and Fe speciation by X-ray

697   Photoelectron Spectroscopy for a crystal full chemical characterization of Ti-Fe Garnet from

698   Colli Albani (Italy) , Annali di Chim., 94(3), 185-196.

699   Schingaro, E., Scordari, F., Mesto, E., Brigatti, M.F. and Pedrazzi, G. (2005) Cation-site

700   Partitioning in Ti-rich micas from Black Hill (Australia): a multi-technical approach. Clays and

701   Clay Minerals, 53(2), 179-189. DOI: 10.1346/CCMN.2005.0530208.

702   Schingaro, E., Lacalamita, M., Scordari, F. and Mesto, E. (2013). 3*T*-Pholgopite from Kasenyi

703   kamafugite (SW Uganda): EPMA, XPS, FTIR AND SCXRD Study. American Mineralogist, in

704   press. DOI: 10.2138/am.2013.4283

705   Scofield, J.H. (1976) Hartree-Slater subshell photoionization cross-section at 1254 and 1487 eV.

706   Journal of Electron Spectroscopy and Related Phenomena, 8, 29. DOI: 10.1016/0368-

707   2048(76)80015-1.

708   Scordari, F., Ventruti, G., Sabato, A., Bellatreccia, F., Della Ventura, G., and Pedrazzi, G. (2006)

709   Ti-rich phlogopite from M.te Vulture (Potenza, Italy) investigated by a multianalytical approach:

710   substitutional mechanisms and orientation of the OH dipoles. European Journal of Mineralalogy,

711   18, 379-391. DOI: 10.1127/0935-1221/2006/0018-0379.

712   Scordari, F., Schingaro, E., Mesto, E. and Lacalamita, M. (2012a). $2M_1$-phlogopite from Black Hills

713   (South Australia): The first case of configurational polytype in micas. American mineralogist,

714   97, 2016-2033. DOI: 10.2138/am.2012.4262.

715   Scordari, F., Schingaro, M., Lacalamita, M. and Mesto, E. (2012b). Crystal chemistry of

716   trioctahedral micas-$2M_1$ from Bunyaruguru (SW Uuganda) Kamafugite. American mineralogist,

717   97, 430-439. DOI: 10.2138/am.2012.3896.

718   Seah, M.P., Gilmore, I.S., Spencer, S.J. (2000) Background subtraction: II. General behaviour of

719   REELS and the Tougaard universal cross section in the removal of backgrounds in AES and

720   XPS. Surface Science, 461, 1-15. DOI: 10.1016/S0039-6028(00)00373-3.

721   Seda, T. and Herne, G. R. (2004) Pressure induced $Fe^{2+}+Ti^{4+} \rightarrow Fe^{3+}+Ti^{3+}$ intervalence charge

722   transfer and the Fe^{3+}/Fe^{2+} ratio in natural ilmenite ($FeTiO_3$) minerals. Journal of Physics:

723   Condensed Matter, 16, 2707-2718. DOI: 10.1088/0953-8984/16/15/022.

724   Seyama, H. and Soma, M. (1985) Bonding-state characterization of the constituent elements of

725   silicate minerals by X-ray photoelectron spectroscopy. Journal of the Chemical Society, Faraday

726   Transactions 1: Physical Chemistry in Condensed Phases, 81, 485-495. DOI:

727   10.1039/F19858100485.

728   Sherman, D.M. (1987) Molecular orbital (SCF-Xα-SW) theory of metal-metal charge transfer

729   processes in minerals. Physics and Chemistry of Minerals, 14(4), 364-367. DOI:

730   10.1007/BF00309811.

731   Sherwood, P.M.A. (1980) Appendix 3 in: D. Briggs, M.P. Seah (Eds.), Practical Surface Analysis

732   by Auger and X-ray Photoelectron Spectroscopy, Wiley, Chichester, 1983.

733   Shirley, D.A. (1972) High-Resolution X-Ray Photoemission Spectrum of the Valence Bands of

734   Gold. Physic Review B, 5, 4709–4714. DOI: 10.1103/PhysRevB.5.4709-4714.

735   Tam, P.L., Cao, Y., Nyborg, L. (2012) XRD and XPS characterisation of transition metal silicide

736   thin films. Surface Science, 606, 329-336. DOI:10.1016/j.susc.2011.10.015.

737   Tougaard, S. (1988a) Quantitative analysis of the inelastic background in surface electron

738   spectroscopy. Surface and Interface Analysis, 11, 453-472. DOI: 10.1002/sia.740110902.

739   Tougaard, S. (1988b) In-depth concentration profile information through analysis of the entire XPS

740   peak shape. Applied Surface Science, 32, 332-337. DOI: 10.1016/0169-4332(88)90018-9.

741   Tougaard, S. (1997) Universality Classes of Inelastic Electron Scattering Cross-sections. Surface

742   and Interface Analysis, 25, 137-154.

743   Tougaard, S. and Sigmund, P. (1982) Influence of elastic and inelastic scattering on energy spectra

744   of electrons emitted from solids. Physic Review B, 25 (7), 4452-4446. DOI:

745   10.1103/PhysRevB.25.4452.

746   Van Veenendoal, M.A. and Sauotzky, G.A. (1993) Nonlocal screening effects in 2p x-ray

747   photoemission spectroscopy core-level line shapes of transition metal compounds. Physical

748   Review letters 70, 2459-2462. DOI: 10.1103/PhysRevLett.70.2459.

749   Waychunas, GA (1987) Synchrotron radiation XANES spectroscopy of Ti in minerals: effects of Ti

750   bonding distances, Ti valence and site geometry on absorption edge structure. American

751   Mineralogist, 72, 89-101.

752   Ventruti, G., Levy, D., Pavese, A., Scordari, F. (2009) High-temperature treatment, hydrogen

753   behavior and cation partitioning of a Fe–Ti bearing volcanic phlogopite by in situ neutron

754   powder diffraction and FTIR spectroscopy. European Journal of Mineralogy, 21, 385-396. DOI:

755   10.1127/0935-1221/2009/0021-1903.

756

757

758

759

760

761

762

763 **Figure captions:**

764 **FIGURE 1.** Curve fits of C1sregion of adventitious carbon on: a) brookite, b) SA mica and c) BHG

765 mica single crystals the background evaluation by Shirley method. The FWHM for all features are

766 1.6, 1.4 and 1.4 eV. for a), b) and c), respectively.

767

768 **FIGURE 2.** Curve fits of the O1s region of: a) brookite, b) SA and c) BHG mica single crystals

769 after that the background evaluation by Shirley method. The FWHM for all features are 1.3, 2.0 and

770 2.0 eV. for a), b) and c) , respectively.

771

772 **FIGURE 3**. Curve fits of the Ti2p region of the reference TiO$_2$ powder after applying six different

773 background subtraction methods. The main peaks are drawn with a solid line while the satellite

774 peaks are depicted with a dashed line. All the peaks of the main doublets were constrained to the

775 same Gaussian/Lorentzian ratio, while the satellites were considered as pure Gaussian peaks.

776

777 **FIGURE 4.** Curve fits of the Ti2p region of the reference single crystal brookite (TiO2) after

778 applying six different background subtraction methods. The main peaks are drawn with a solid line

779 while the satellite peaks are depicted with a dashed line. All the peaks of the main doublets were

780 constrained to the same Gaussian/Lorentzian ratio, while the satellites were considered as pure

781 Gaussian peaks.

782

783 **FIGURE 5a**. Curve fits of the Ti2p region of the reference single crystal mica (SA) after applying

784 six different background subtraction methods.

785

786   **FIGURE 5b**. Curve fits of the Fe2p region of the reference single crystal mica (SA) after applying

787   six different background subtraction methods. The Fe^{2+} multiplet components are drawn with thick

788   solid lines, Fe^{3+} multiplet components with a thin solid lines and satellite peaks with dotted lines. In

789   the inset a zoom of the satellite region as evaluated by background removal with "Shape parameter,

790   k" method is shown.

791

792   **FIGURE 6a**. Curve fit of the Ti2p region using a mica single crystal (BHG) after the background

793   was evaluated by "Shape parameter, κ" method.

794

795   **FIGURE 6b**. Curve fit of the Fe2p region using a mica single crystal (BHG) after the background

796   was evaluated by "Shape parameter, κ" method. The Fe^{2+} multiplet components are drawn with

797   thick solid lines, Fe^{3+} multiplet components with a thin solid lines and satellite peaks with dotted

798   lines.
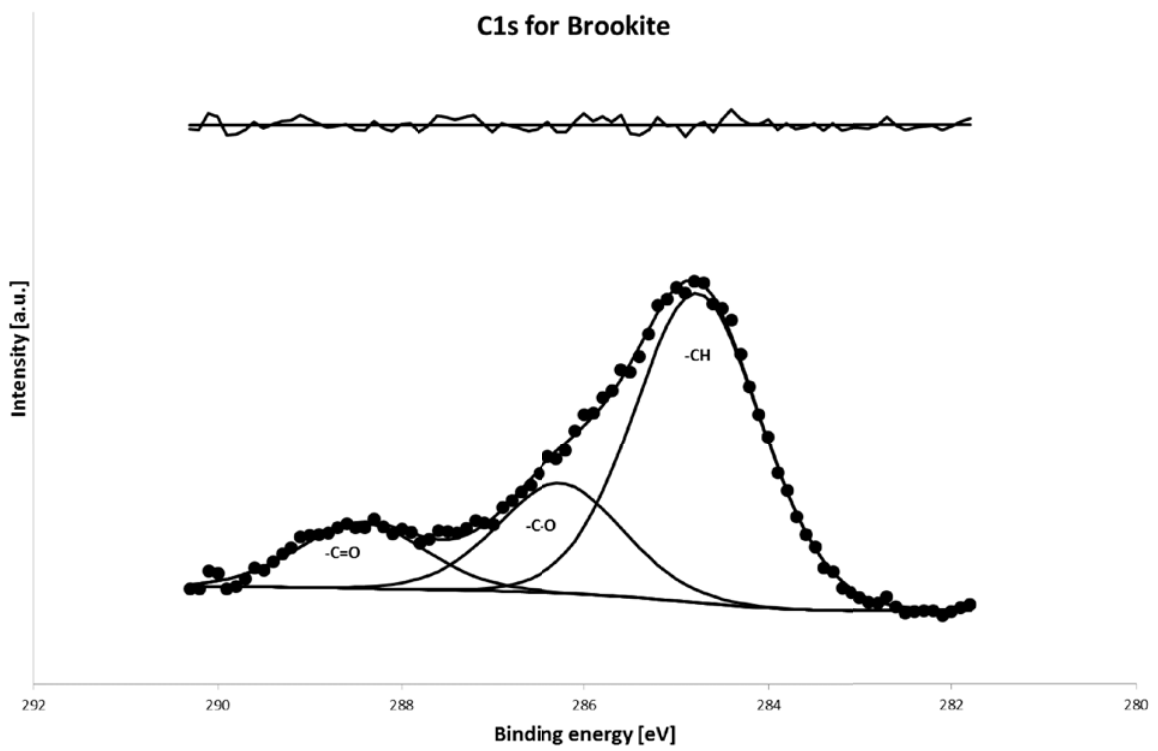
Figure 1a
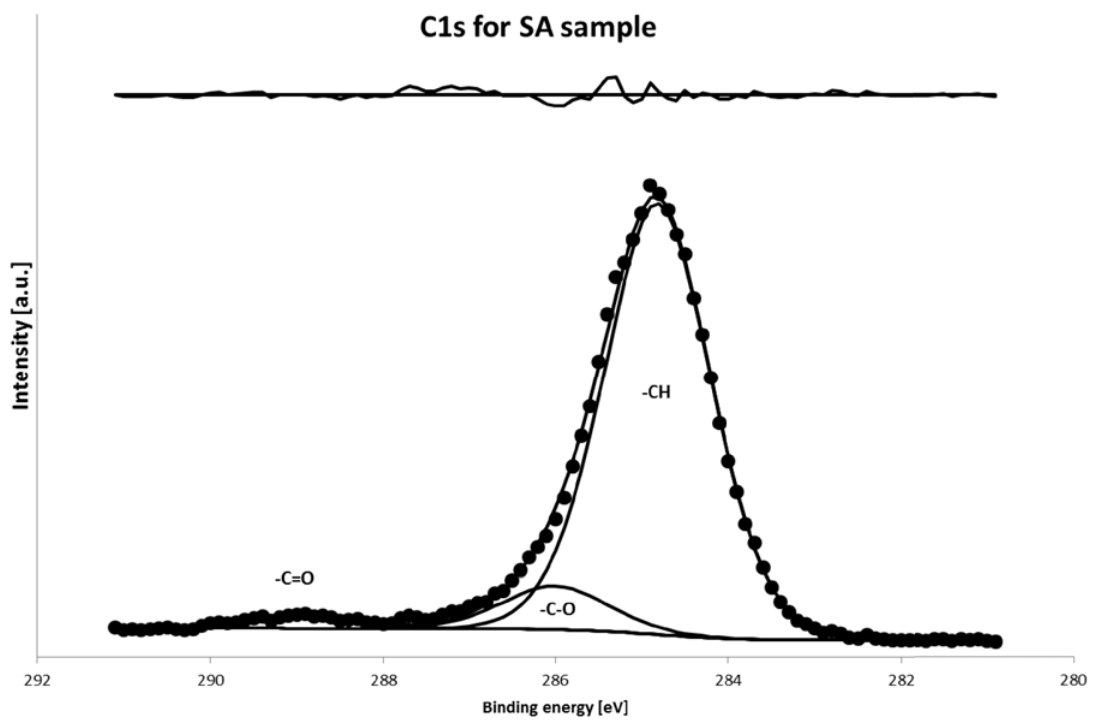
Figure 1b
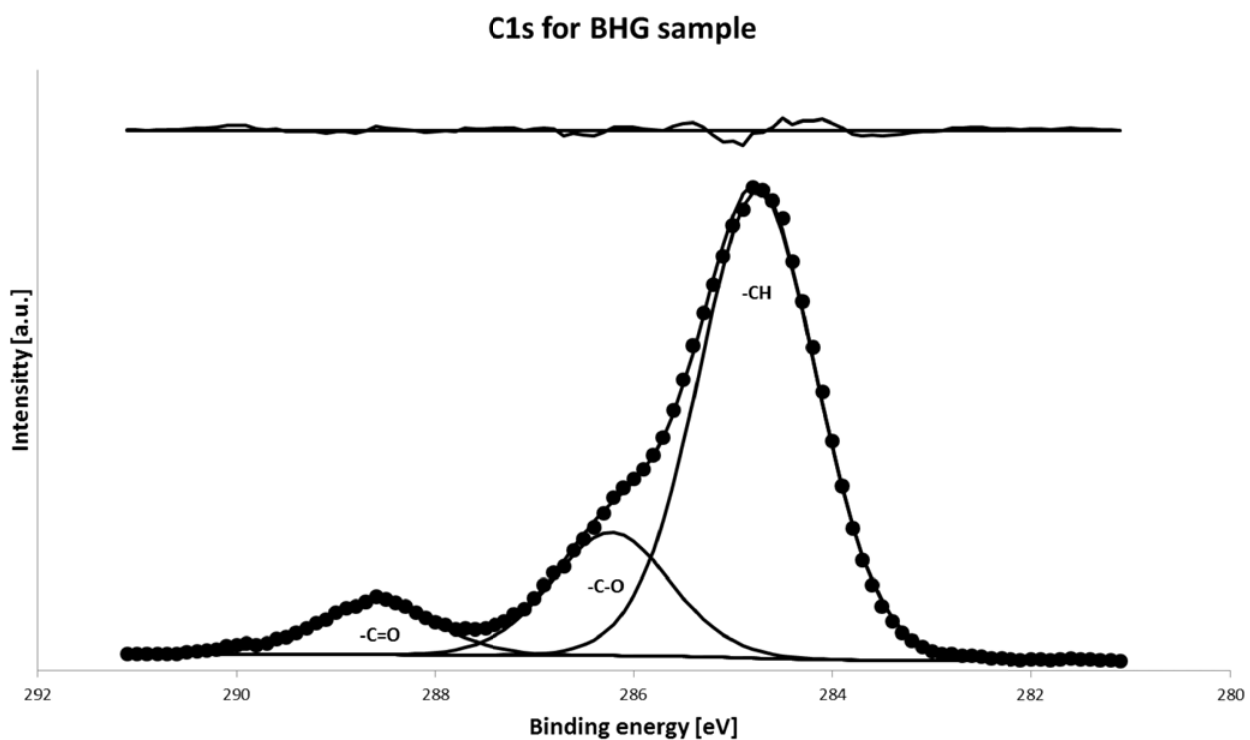
Figure 1c
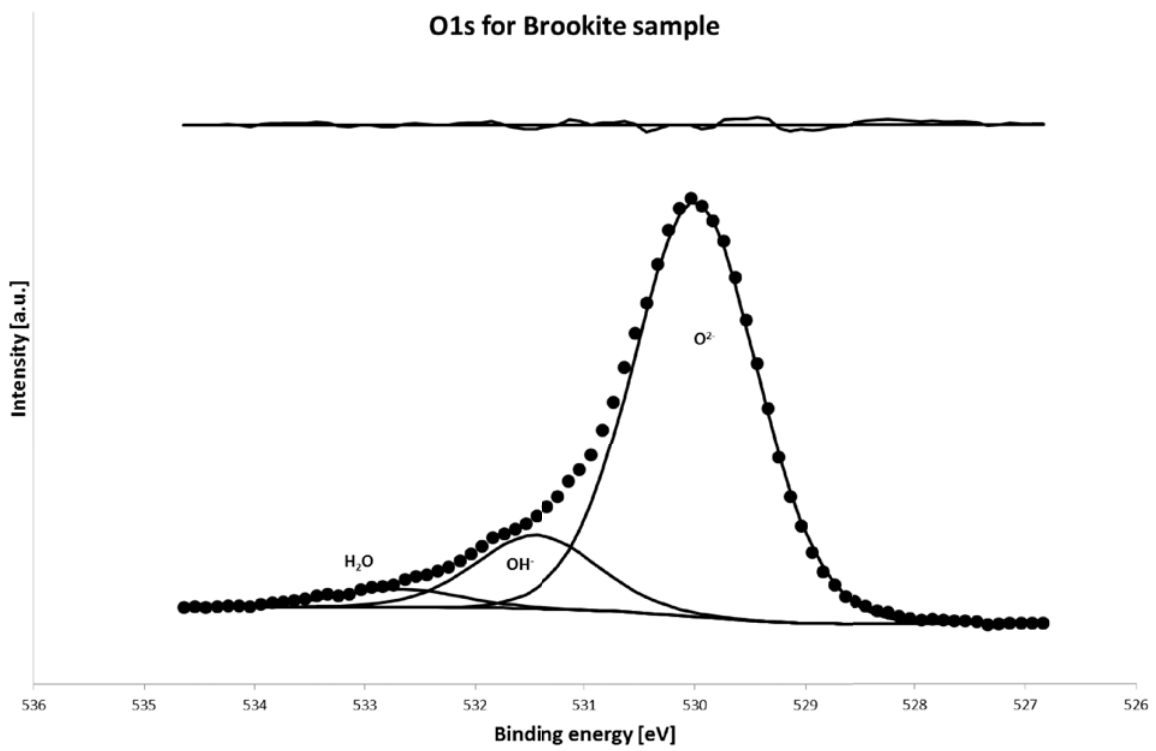
Figure 2a
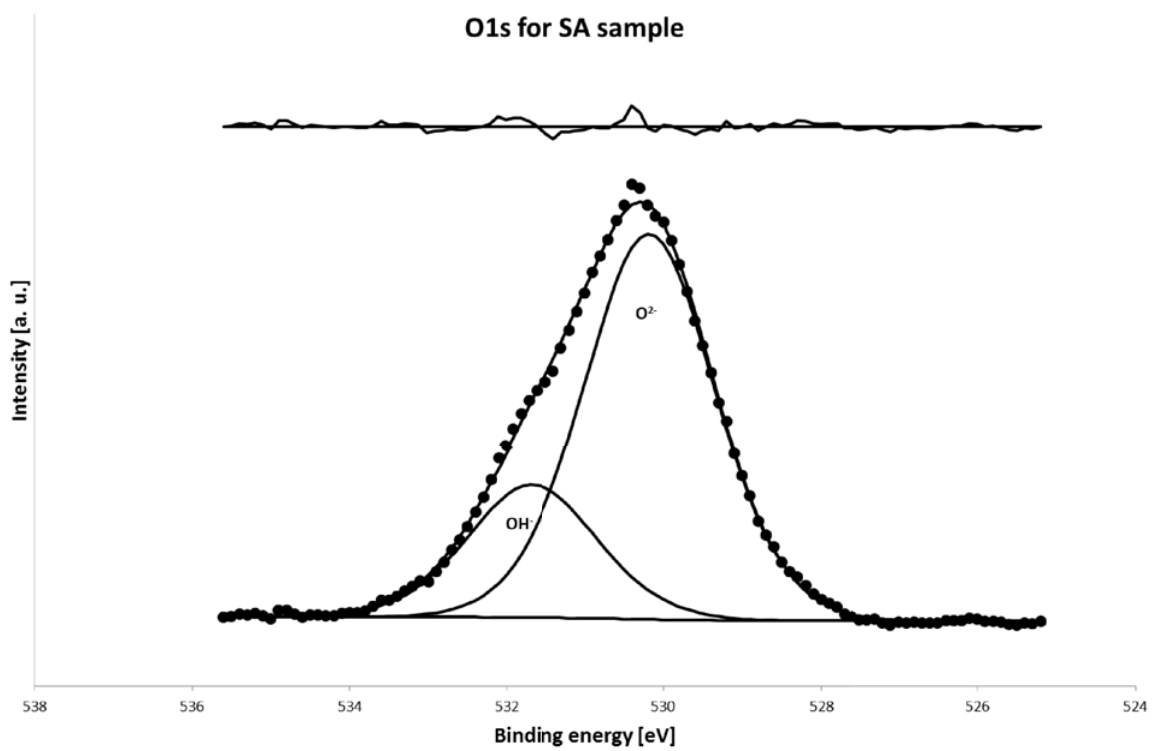
Figure 2b
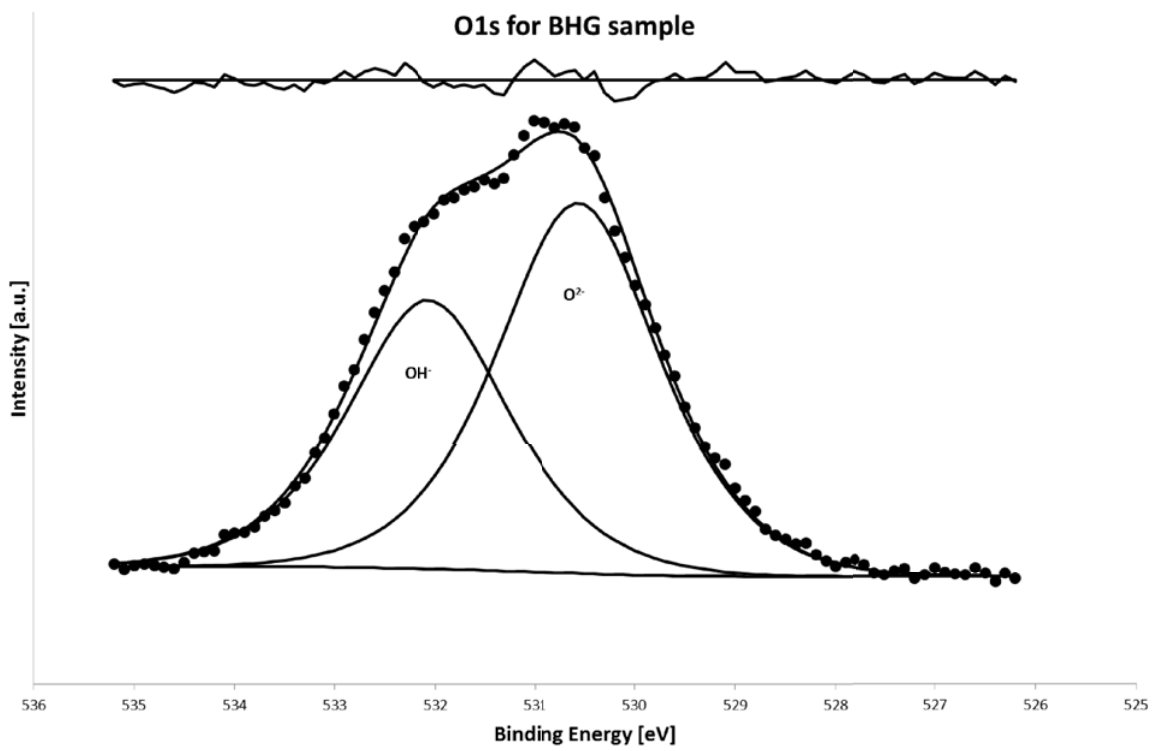
Figure 2c
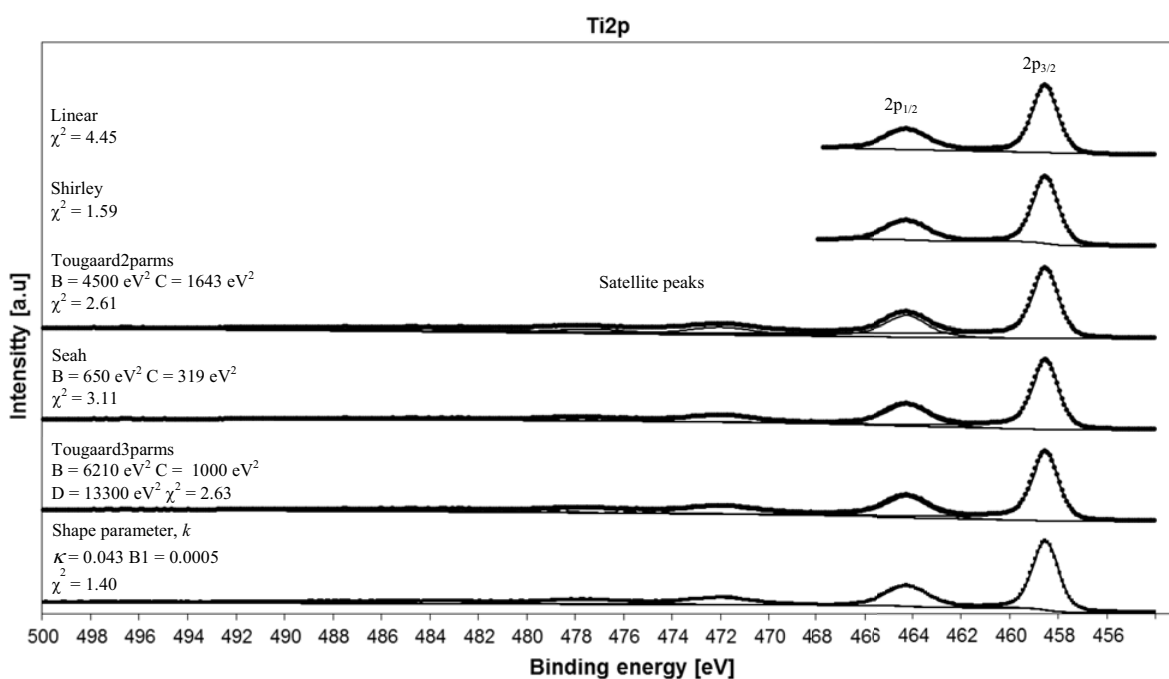
Figure 3.
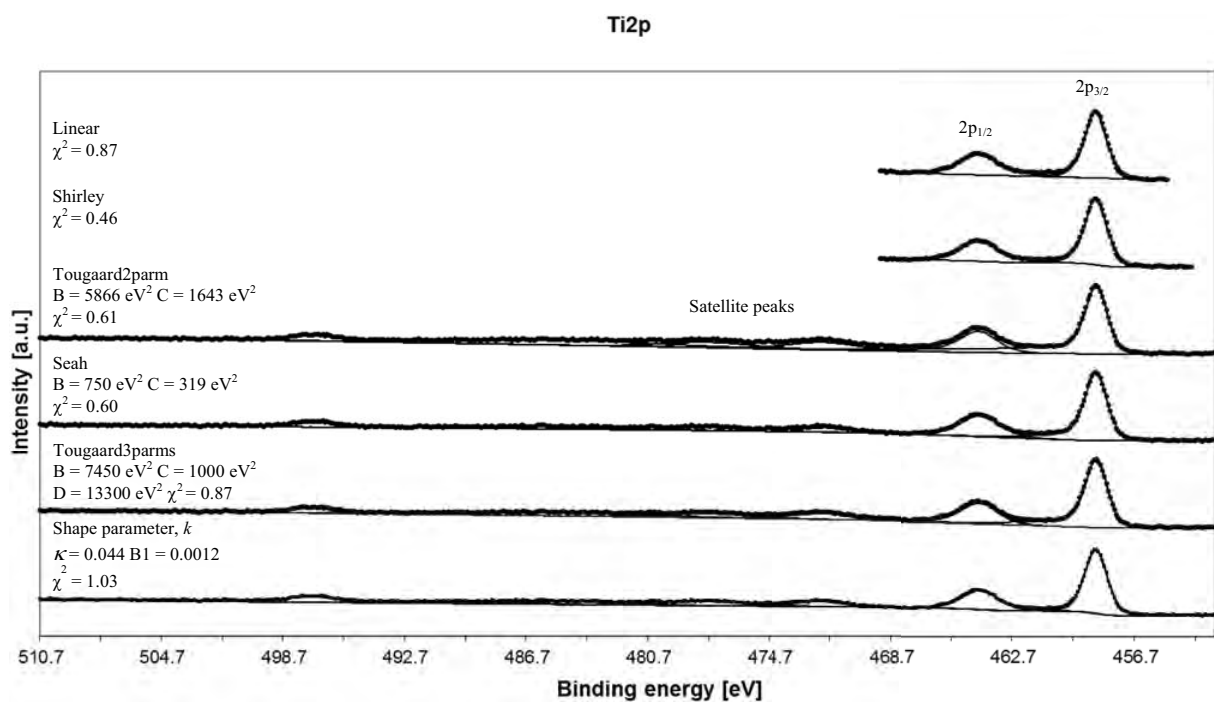
Figure 4.
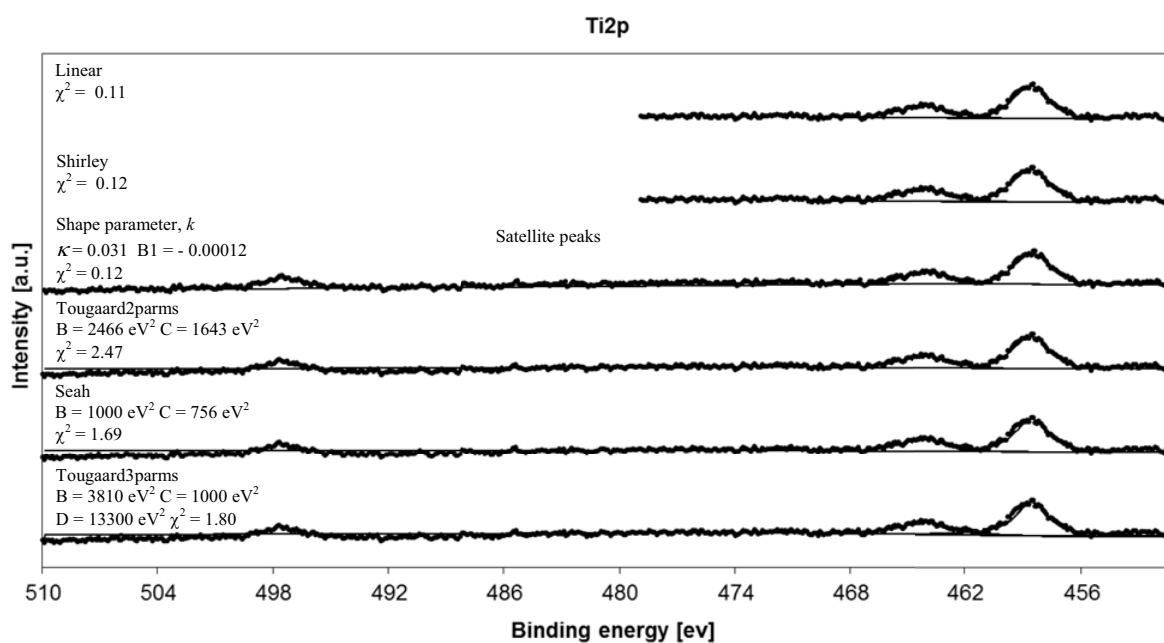
Figure 5a.
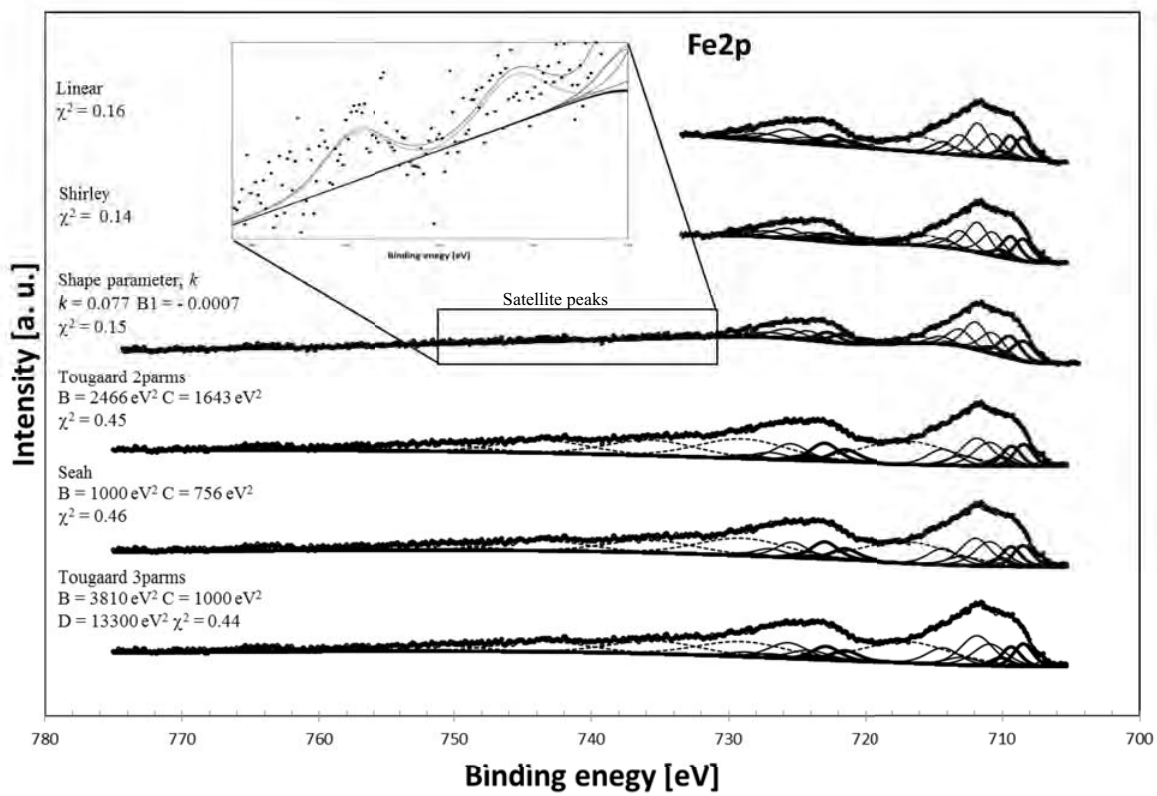
Figure 5b.
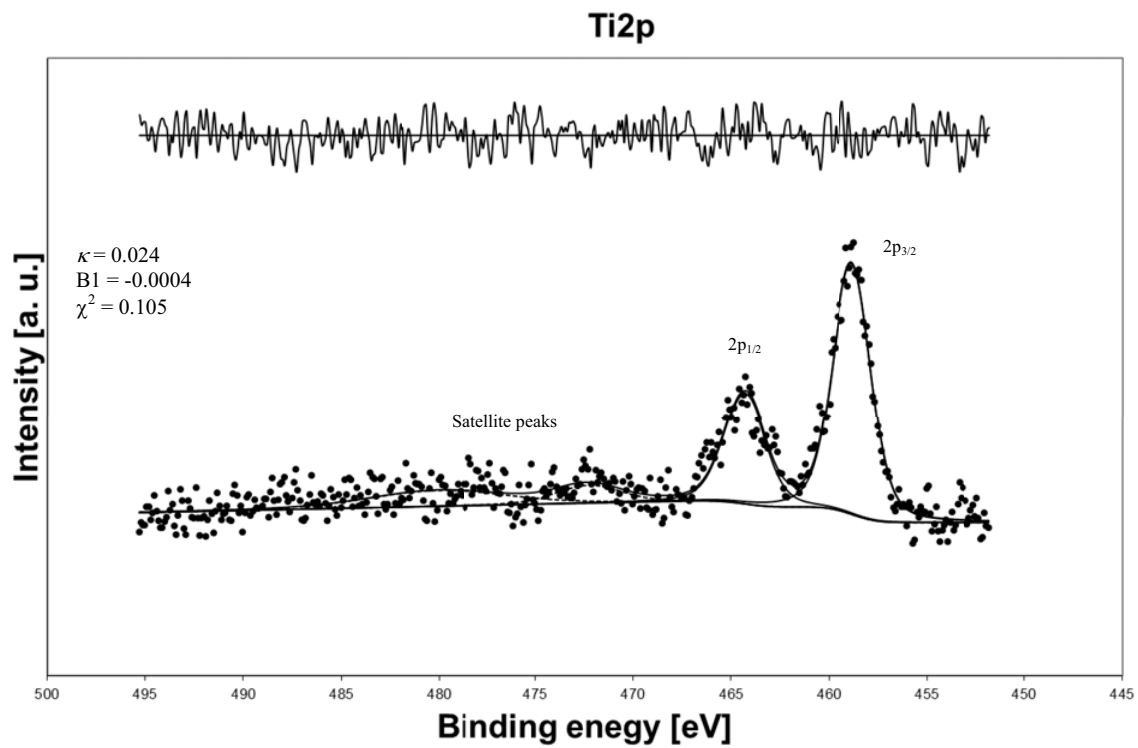
Figure 6a.
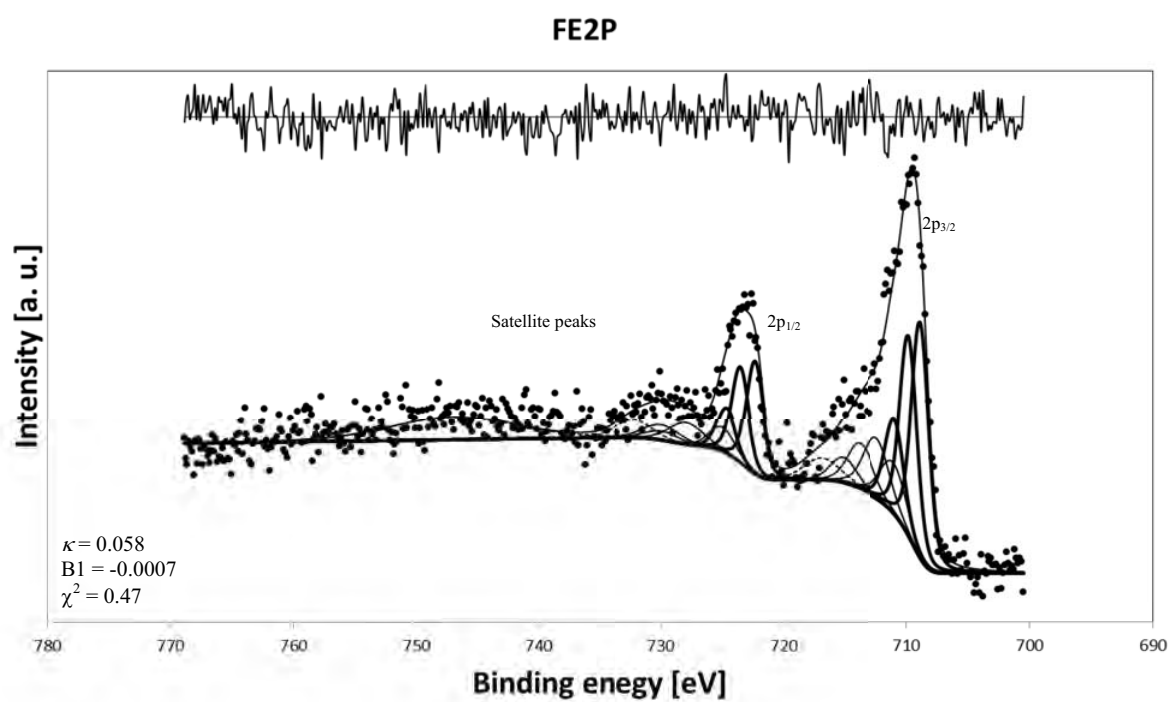
Figure 6b.

Table 1. Results of the Ti2p curve fit for synthetic TiO_2 oxide powder and natural brookite (TiO_2).

	TiO₂ powder					
	Linear	**Shirley**	**Tougaard2parms**	**Seah**	**Tougaard3parms**	**Shape parameter, κ**
BE 2p$_{3/2}$ (eV)	458.62	458.58	458.57	458.57	458.58	458.59
2p$_{3/2}$ FHWM (eV)	1.25	1.24	1.22	1.21	1.22	1.26
BE 2p$_{1/2}$ (eV)	464.26	464.25	464.31	464.27	464.29	464.27
2p$_{1/2}$ FHWM (eV)	2.33	2.06	2.09	2.09	2.08	2.08
	Brookite					
	Linear	**Shirley**	**Tougaard2parms**	**Seah**	**Tougaard3parms**	**Shape parameter, κ**
BE 2p$_{3/2}$ (eV)	457.95	457.93	457.9	457.9	457.9	457.93
2p$_{3/2}$ FHWM (eV)	1.27	1.32	1.29	1.29	1.29	1.32
BE 2p$_{1/2}$ (eV)	463.63	463.61	463.69	463.61	463.64	463.62
2p$_{1/2}$ FHWM (eV)	2.43	2.29	2.2	2.2	2.18	2.14

Table 2. Results of the Ti2p and Fe2p curve fit for SA mica.

	SA mica					
Ti^{4+}						
	Linear	**Shirley**	**Tougaard2parms**	**Seah**	**Tougaard3parms**	**Shape parameter, κ**
BE 2p$_{3/2}$ (eV)	458.63	458.64	458.58	458.63	458.63	458.65
2p$_{3/2}$ FHWM (eV)	2.31	2.42	2.16	2.34	2.37	2.30
BE 2p$_{1/2}$ (eV)	464.23	464.26	464.24	464.21	464.20	464.26
2p$_{1/2}$ FHWM (eV)	3.27	3.00	2.50	2.95	3.24	2.75
Fe^{3+}						
	Linear	**Shirley**	**Tougaard2parms**	**Seah**	**Tougaard3parms**	**Shape parameter, κ**
BE 2p$_{3/2}$ (eV) Peak 1	710.4	710.69	710.90	710.88	710.90	710.53
2p$_{3/2}$ FHWM (eV)	2	2.00	2.79	2.79	2.92	2.03
BE 2p$_{3/2}$ (eV) Peak 2	711.8	711.80	711.84	711.80	711.82	711.91
2p$_{3/2}$ FHWM (eV)	2	2.00	2.79	2.79	2.92	2.03
BE 2p$_{3/2}$ (eV) Peak 3	713.03	713.05	712.90	712.95	721.90	713.11
2p$_{3/2}$ FHWM (eV)	2	2.00	2.79	2.79	2.92	2.03
BE 2p$_{3/2}$ (eV) Peak 4	714.3	714.30	714.30	714.30	714.30	714.51
2p$_{3/2}$ FHWM (eV)	2	2.00	2.79	2.79	2.92	2.03
BE 2p$_{1/2}$ (eV) Peak 1	724.28	724.00	723.88	724.33	724.17	724.20
2p$_{1/2}$ FHWM (eV)	2.36	2.80	3.09	3.09	3.50	2.20
BE 2p$_{1/2}$ (eV) Peak 2	727.13	725.72	725.49	725.59	725.67	725.70
2p$_{1/2}$ FHWM (eV)	2.36	2.80	3.09	3.09	3.50	2.20
BE 2p$_{1/2}$ (eV) Peak 2	728.7	727.18	727.00	727.00	727.00	727.10

2p$_{1/2}$ FHWM (eV)	2.36	2.80	3.09	3.09	3.50	2.20
BE 2p$_{1/2}$ (eV) Peak 2	729.2	728.38	727.70	728.70	728.70	727.10
2p$_{1/2}$ FHWM (eV)	2.36	2.80	3.09	3.09	3.50	2.20

Fe^{2+}						
	Linear	**Shirley**	**Tougaard2parms**	**Seah**	**Tougaard3parms**	**Shape parameter, κ**
BE 2p$_{3/2}$ (eV) peak 1	708.48	708.47	708.45	708.41	708.46	708.46
2p$_{3/2}$ FHWM (eV)	1.36	1.62	1.70	1.70	1.70	1.84
BE 2p$_{3/2}$ (eV) peak 2	709.4	709.37	709.32	709.37	709.35	709.43
2p$_{3/2}$ FHWM (eV)	1.36	1.62	1.70	1.70	1.70	1.84
BE 2p$_{3/2}$ (eV) peak 3	710.4	710.70	710.90	710.92	710.70	710.71
2p$_{3/2}$ FHWM (eV)	1.36	1.62	1.70	1.70	1.70	1.84
BE 2p$_{1/2}$ (eV) peak 1	721.8	721.80	721.50	721.65	721.50	721.74
2p$_{1/2}$ FHWM (eV)	3.49	2.72	2.50	2.50	2.50	2.00
BE 2p$_{1/2}$ (eV) peak 2	722.94	722.80	0.00	723.00	722.90	722.74
2p$_{1/2}$ FHWM (eV)	3.49	2.72	2.50	2.50	2.50	2.00
BE 2p$_{1/2}$ (eV) peak 1	723.5	723.50	723.88	723.88	723.60	723.54
2p$_{1/2}$ FHWM (eV)	3.49	2.72	2.50	2.50	2.50	2.00

Table 3. Results of the Ti2p and Fe2p curve fit for BHG mica evaluating the background with the "shape parameter, κ" method. All the peaks of the main doublets were constrained to the same Gaussian/Lorentzian .

	Ti^{4+}	Fe^{2+}			Fe^{3+}			
		Peak 1	Peak 2	Peak 3	Peak 1	Peak 2	Peak 3	Peak 4
BE $2p_{3/2}$ (eV)	458.80	708.89	709.85	710.99	711.09	712.49	713.79	715.19
$2p_{3/2}$ FHWM (eV)	2.30	1.64	1.64	1.64	2.50	2.50	2.50	2.50
BE $2p_{1/2}$ (eV)	464.30	722.46	723.66	724.76	725.06	727.96	729.96	730.00
$2p_{1/2}$ FHWM (eV)	2.50	1.64	1.64	1.64	3.00	3.00	3.00	3.00